

## EXPERIMENTAL STUDIES OF BRICK AND MORTAR COMPOSITES USING DIGITAL IMAGE ANALYSIS

AMIR H. MOHAMMADIPOUR<sup>\*</sup>, KASPAR J. WILLAM<sup>†</sup>, ASHRAF AYOUB<sup>#</sup>

<sup>\*</sup> University of Houston  
Department of Civil and Environmental Engineering,  
N110 Engineering Building 1, Houston, TX, USA  
Email: [amohammadipour@uh.edu](mailto:amohammadipour@uh.edu)

<sup>†</sup> University of Houston  
Department of Civil and Environmental Engineering,  
N110 Engineering Building 1, Houston, TX, USA  
Email: [kwillam@uh.edu](mailto:kwillam@uh.edu)

<sup>#</sup> University of Houston  
Department of Civil and Environmental Engineering,  
N110 Engineering Building 1, Houston, TX, USA  
Email: [asayoub@uh.edu](mailto:asayoub@uh.edu)

**Key words:** Masonry Prism, Brick, Mortar, Uniaxial Compression, Digital Image Correlation, ARAMIS.

**Abstract:** The contribution presents novel observations on unreinforced masonry made of solid clay brick units and surrounding mortar joints. Focus is the brittle-ductile interaction of the two constituents in form of the so-called masonry prism test under axial compression. The experimental observations include Digital Image Correlation (DIC) data from a newly acquired 3-D DIC system to ascertain the effect of bond on the overall behaviour of the masonry composite. Special attention is directed towards the use of the DIC system to observe mismatch among the two constituents leading to tensile splitting under axial compression. Preliminary tests were performed on the brick units and mortar cubes aside from the masonry prisms using the 3-D DIC system for imaging which did display interesting results which would have been missed by traditional deformation measurements. The presentation concludes with remark on the resolution and limitations of the DIC system.

### 1 INTRODUCTION

Masonry walls are widely used in building constructions around the world for its low cost material and broad availability, and its sound insulation properties and energy efficiency. Unreinforced masonry is a heterogeneous, inelastic, and anisotropic material made of two components, brick units and mortar joints exhibiting very different stiffness, strength and ductility properties. When these two constituents are assembled in form of a

masonry prism, a stack of bricks bonded by mortar bed joints, axial splitting of the prism is observed under compressive loading due to the mismatch conditions of the masonry composite. This mismatch results from the different response behaviour of the stiff brick units and the soft mortar layers generating triaxial stress and deformation conditions in the brick unit and the mortar joint. This means that during axial compression of the masonry prism the softer mortar joints are restrained by the brick units from lateral expansion and

hence experience triaxial confinement, while the stiffer brick units are subjected to lateral tension besides far-field axial compression.

A number of investigations have been conducted on different aspects of masonry and the interface behavior between brick and mortar joints [ (1), (2), (3), (4), (5), (6), (7)]. Goodman et al. (1) were one of the first researchers who introduced the interface concept for joints in rock mechanics. Their joint element was designed to feature failure in tension and/or shear, rotation of blocks, development of arches. Page (2) of their seminal paper analyzed the behavior of clay masonry walls subjected to in-plane loading using an early version of degenerate finite elements. The model considered masonry as a continuum of isotropic elastic bricks acting in concert with mortar layers as joint linkage elements. However, the ultimate load capacity of the masonry could not be predicted at that early stage. McNary and Abrams (3) studied biaxial tension-compression of bricks and triaxial compression of mortar to establish constitutive relations for each material. They simulated the force-deformation relationship for a stack-bond prism using a numerical model and a proposed strength theory. They concluded that mechanics of clay-unit masonry in compression could be represented by a single failure model and the most significant parameter to consider was the dilatant behaviour of the mortar. Blackard et al. (5) investigated the fundamental meso-mechanical failure processes in masonry prisms under axial compression. They emphasized that 3-D analysis is more realistic than a 2-D plane stress analysis which significantly underestimates the compression capacity of the masonry prism. They concluded that the out-of-plane confinement plays a critical role in the assessment of the overall compression capacity of masonry walls, where 2-D generalized plane strain analysis is more realistic than plane strain and plane stress. Citto et al. (7) employed an innovative approach using digital image correlation (DIC) techniques to evaluate in-situ properties of the shear strength of mortar joints in existing masonry. They determined in

the properties of cohesion and friction angles in an existing masonry wall, and they used finite elements and the DIC system to investigate the significant lack of uniformity along the bed joints failing in shear.

This paper focuses on recent experimental observations of fired clay bricks and mortar specimens at the constituent levels, in addition to their composite behaviour when brick and mortar are assembled and tested in compression. The experimental observations include digital image correlation (DIC-GOM) data from a newly acquired 3-D system to ascertain the effect of bond on the overall behaviour of the masonry composite.

## 2 DIGITAL IMAGE CORRELATION SYSTEM

For image analysis, the Digital Image Correlation system ARAMIS from GOM (2) was used in all experiments. In the DIC technique, the software processes the images taken during the test to determine the full-field motion of the speckle geometry and determines surface deformations in terms of strain measurements. The DIC setup used for this study, is a non-contact optical 3D metrology system in which the ARAMIS software analyzes, calculates and documents deformations at prescribed load steps (2). The setup consists of four pairs of 12 megapixel Gigabit Ethernet cameras connected to a sensor controller for power supply of the cameras and to record speckle images in pixel format. The PC-based ARAMIS software assigns square or rectangular image details in form of so-called facets, e.g. 15 x 15 pixels, for tracking their motion over the deformation history of the test article. a

There are steps to accomplish in a typical measuring procedure (2), some of which are related to specimen preparation, calibration of the measuring volume, creating a new project and defining its parameters like facet size, facet steps, computation size (gauge length) and so forth. In order to measure a specimen's deformation using ARAMIS system, its surface facing towards the cameras must meet some requirements like being smooth, having

a stochastic pattern with good contrast to clearly allocate the pixels in the camera images (facets), being non-glossy and dull, being free of grease and oil, etc. In this experimental investigation, a plain spray paint from Wal-Mart was used to create stochastic patterns on the specimen surface. Satin or gloss paints were avoided because of their reflections under lighting. First, a white and dull base coat was applied on the specimen's surface followed by spraying black random dots to generate a speckle pattern. Smaller measuring volumes require a finer pattern than large measuring ones. Figure 1 shows a standard masonry prism prepared with a random dot pattern in this study.

### 3 LABORATORY TESTS

In the present study, three types of specimens were considered, sintered clay brick units without holes, mortar cubes, and five-brick standard masonry prisms. As explained earlier, when the masonry prism is under axial compression, the mortar joints experience triaxial compression while the brick units are subjected to axial compression and lateral biaxial tension due to the mismatch properties of mortar and brick units. Softer mortar joints generate lateral tension in the bricks through their interface bond leading to tensile cracking in form of axial splitting of the brick units. This mode-I failure initiates in the brick units and propagates through mortar joints. Since the brick is in both tension and compression, its tensile and compressive strengths and its failure mode are of particular interest. The



**Figure 1:** Stochastic patterns sprayed on a masonry prism surface.

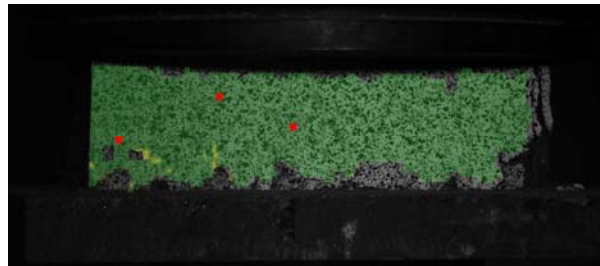
compressive strength of the mortar cube was investigated under axial compression. A Tinius-Olsen axial tension-compression material testing machine was used with maximum capacity of 400 kips for all tests in this experimental investigation. Also, the DIC system was used for all tests to capture the full-field deformation of test specimens at different load stages of axial displacement control.

#### 3.1 Fired clay brick units

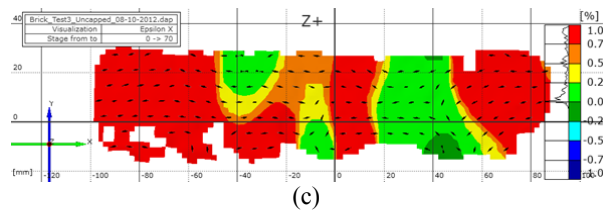
The solid brick units of nominal size 2x4x8 in were acquired from a well-known local company in Houston, Texas. Three randomly selected bricks were used for compression and



(a)



(b)



(c)

**Figure 2:** Brick specimen under uniaxial compression at the load level of 180 kips ( $0.87P_{max}$ ). (a) The brick with speckles, (b) The snapshot taken by the DIC software, (c)  $\epsilon_x$  contours on the surface of the brick.

three for splitting tension (Brazilian) tests. The splitting tension test complies with the specifications of ASTM C 1006-84 (3). Figure 2 shows the typical brick specimens painted and prepared for the compression test.

Figure 2(a) and Figure 2(b) illustrate the speckles on the surface of a tested brick taken by a regular camera and DIC software, respectively. Figure 2(c) shows the distribution of  $\varepsilon_x$  contours on the brick's surface shown in Figure 2(a). The dark green contours correspond to lateral contraction, i.e. negative  $\varepsilon_x$  strain values contradicting the Poisson effect. However, this may be explained by the boundary effects at the two brick surfaces. Other colors are related to different levels of lateral tensile strain.

Moreover, splitting tension tests were conducted on three brick units, since the brick commonly fails in tensile mode in a masonry assemblage. In the test, two line loads along the bed surfaces of the brick were applied. The compressive load was imposed by 0.25" in diameter bearing rods, results in a tensile stress distributed over the height of the brick over the split length of the unit. The splitting tensile strength of the bricks is calculated according to the traditional expression for split tensile testing as:

$$T = \frac{2P}{\pi LH} \quad (1)$$

where:

$T$  = splitting tensile strength, psi (kPa),

$P$  = maximum applied load indicated by the testing machine, lb (kN),

$L$  = split length (width) of the brick, in. (m),

$H$  = height of the brick, in. (m).

The average splitting tensile strength for the three bricks was 0.407 ksi, which is close to a typical value of concrete.

Figure 3 illustrates the splitting tension test performed on one brick. Figure 3(a) shows the painted brick after the test with a vertical mode I crack through its height. Figure 3(b) shows the photo taken by the DIC system right after the failure, while Figure 3(c) shows the distribution of  $\varepsilon_x$  and major principal strains'

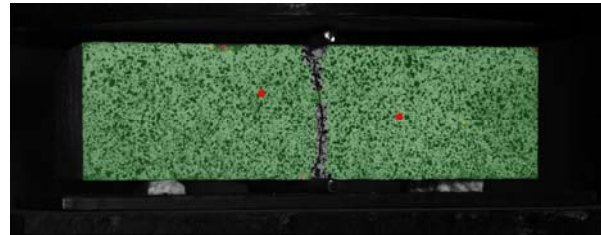
directions on the surface of the brick right before the failure. As it can be seen, there are strain concentrations (red colors) right below and above the bearing rods on the middle top and bottom of the brick. This coincides with what is expected in the Brazilian test setup. Other parts of the brick surface are almost free of deformations showing green color.

### 3.2 Mortar cubes

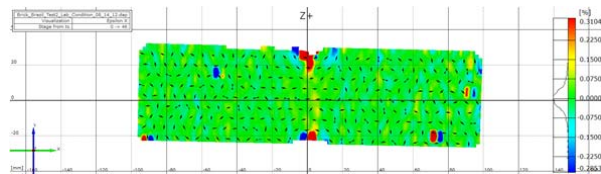
Mortar mixture was prepared with a 4:1 sand to cement ratio and a W/C ratio of 0.56



(a)

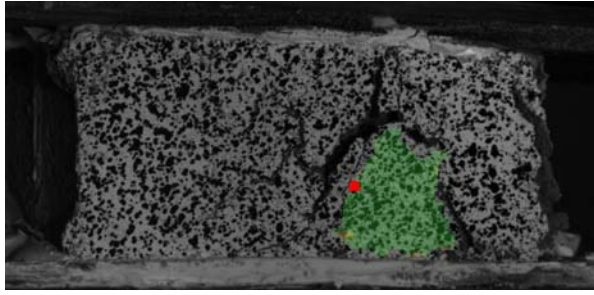


(b)

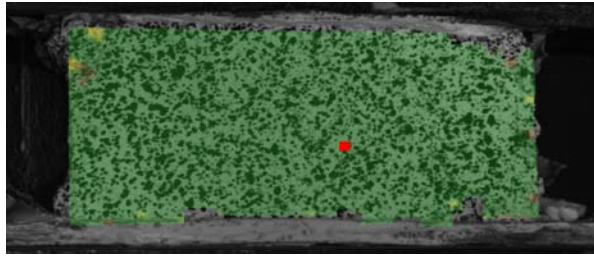


(c)

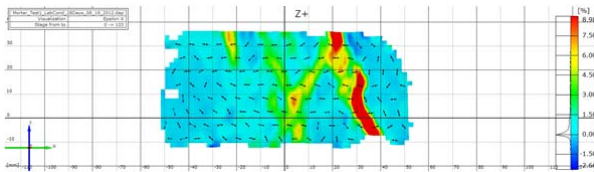
**Figure 3:** Brick specimen in splitting tension test failed at the load level of 6.1 kips. (a) The brick with speckles after the test, (b) The snapshot taken by the DIC software right after the failure, (c)  $\varepsilon_x$  contours on the surface of the brick right before the tensile splitting.



(a)



(b)



(c)

**Figure 4:** Mortar cube specimen cured for 28 days under uniaxial compression at the load level of 40.9 kips ( $0.97P_{max}$ ). (a) The mortar after failure, (b) The snapshot taken by the DIC software at  $0.97P_{max}$ , (c)  $\epsilon_x$  contours on the surface of the mortar  $0.97P_{max}$ .

for the entire experimental test program. The mixture was formed as a cube surrounded by brick surfaces the dimension of which was 4'' x 4'' x 2''. The mortar cubes were cured for 14 and 28 days inside a moisture-tight bag. The

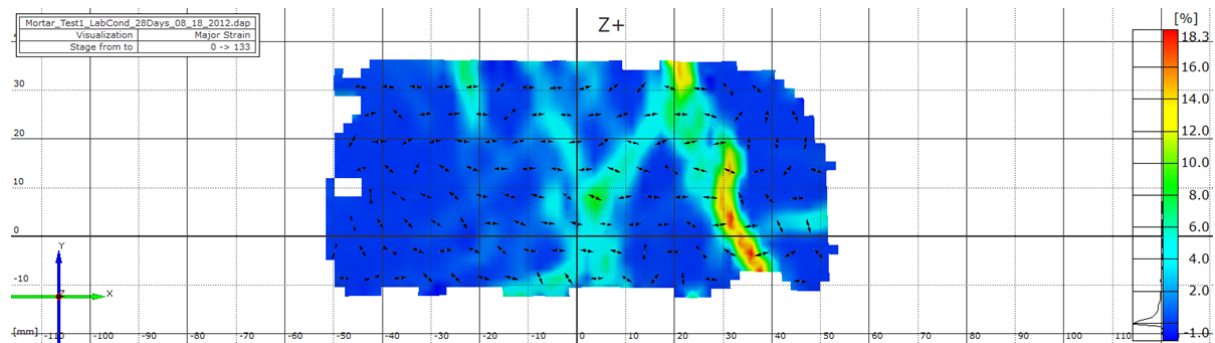


**Figure 5:** Major strain distribution and its direction on the surface of the mortar cube at  $0.97P_{max}$  captured by the DIC system.

cubes were tested in axial compression under displacement control test at the same displacement rate as the brick units.

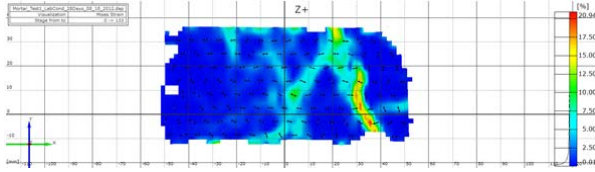
Figure 4 illustrates a mortar cube tested in this study under axial compression. Figure 4(b) and (c) show the mortar very close to its failure. As can be seen, the DIC software can capture the strain concentrations on the surface of the specimen. If Figure 4(a) is compared with Figure 4(c), it is evident that the fracture trajectory closely matches with the one for  $\epsilon_x$  concentration.

Figure 5 shows the distribution of the major strain distribution and its directions along the surface of the same mortar shown in Figure 4. Viewing Figure 4(a) and Figure 5, we may conclude that the ARAMIS system can locate the crack path 'before failure' by measuring the increasing rate of localized deformations.

Attention should also be paid to the principal strains. Figure 5 depicts the direction of the major principal strains which are oriented perpendicularly to the trajectory of the strain concentrations. To explore also whether the failure mode is I or II type, one might look at the von Mises strain contours as depicted in Figure 6. It is observed that there are also high von Mises strains at the location of cracks. This means that the axial fracture mechanisms are a combination of Mode I and Mode II, or a mixed mode failure condition.

### 3.3 Masonry prisms

The masonry prisms were made of five brick units from the same source as used in section 4.1 and four mortar layers from the same cement and aggregates and mix proportions. They were constructed according



**Figure 6:** Mises strain distribution on the surface of the mortar cube at  $0.97P_{max}$  captured by the DIC system.

to the specifications of ASTM C 1314 – 03b (4). Figure 1 shows a typical masonry prism prepared for this study the height of which is 12 in. The prisms were tested under a uniaxial compression in displacement control with the same displacement rate as the brick units' and mortar cubes'.

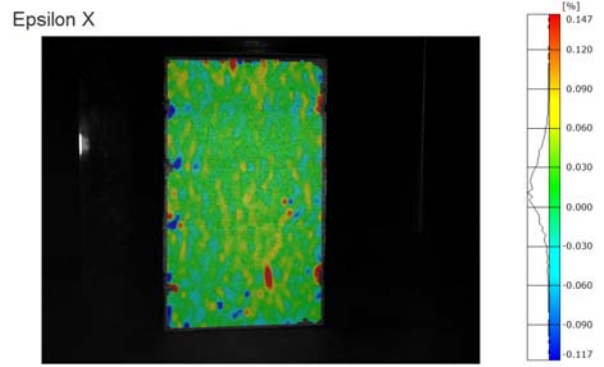
Figure 7(a) and (b) illustrate the distribution of  $\epsilon_x$  contours at the load level of 88 and 171 kips, respectively. In Figure 7(a), most of the lateral strain field (see the strain bar) exhibits positive  $\epsilon_x$ -values with some vertical strain concentrations having been developed (yellow color).

Figure 7(b) shows the development of a vertical crack at failure. The DIC system captures the concentrations of lateral strain depicting the axial crack location and orientation. If the propagation history of the crack evolution is considered, we may observe that the vertical crack propagates from the bottom to the top of the masonry prism in this case. The crack initiates at a load level of 35 kips at the lowest mortar layer somewhere at the brick-mortar interface (about 2.4 in. from the bottom of the prism), and then propagates upward under increasing load until the prism splits into two parts.

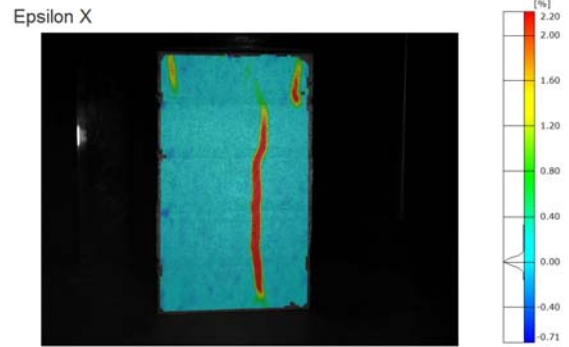
Moreover, to observe the effect of interface shear of the brick-mortar contact zone which is caused by the mismatch effects explained in section 2, the von Mises strain criterion was considered:

$$\epsilon_M = \sqrt{\frac{1}{2}[(\epsilon_1 - \epsilon_2)^2 + (\epsilon_2 - \epsilon_3)^2 + (\epsilon_3 - \epsilon_1)^2]} \quad (2)$$

Where  $\epsilon_1$ ,  $\epsilon_2$ , and  $\epsilon_3$  are major principal strains and  $\epsilon_M$  is the von Mises strain. Figure 8 illustrates the distribution of  $\epsilon_M$  on the surface



(a)



(b)

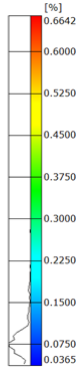
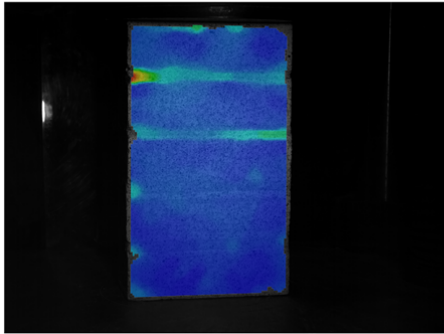
**Figure 7:** Distribution of  $\epsilon_x$  on the surface of the masonry prism during the uniaxial compression test. (a)  $\epsilon_x$  contours at  $0.5P_{max}$ , (b)  $\epsilon_x$  contours at  $P_{max}$ .

of the masonry prism during the uniaxial compression test as captured by the DIC system. Figure 8(a) shows the prism after failure. A comparison can be made between Figure 8(a) and Figure 8(c) or Figure 7(b). It is seen that the DIC system measures the deformations in real-time during the test and at the end it captures the real crack pattern of axial splitting. This provides the DIC system a servo-controlled capability to give feedback to the testing machine by a real time measurement of the deformations. Unfortunately, the testing machine used in this study, i.e. The Tinius Olsen, does not have the capability of a real-time testing, however, a newly purchased test frame has modern feedback control which will be delivered to the University of Houston in the near future, by which crack-opening displacement control testing might be conducted by incorporating virtual clip gauges in the DIC software IVIEW.



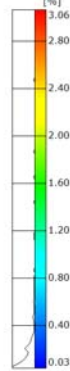
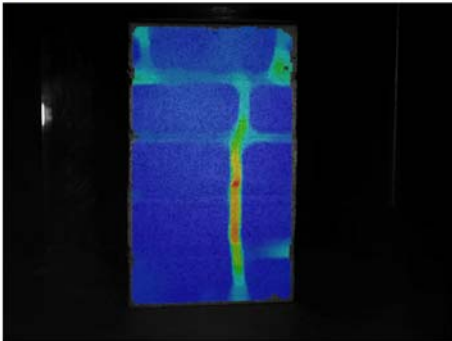
(a)

Mises Strain



(b)

Mises Strain



(c)

**Figure 8:** Distribution of  $\epsilon_M$ , Mises strain, on the surface of the masonry prism during the uniaxial compression test.

(a) The failed masonry prism after the uniaxial compression test. (b)  $\epsilon_M$  contours at  $0.5P_{max}$ , (c)  $\epsilon_M$  contours at  $P_{max}$ .

As expected, the softer mortar layers experience higher shear strains than the stiffer bricks. This is evident in Figure 8(b) and (c) where a lighter blue color is seen at the top mortar layer at  $0.5P_{max}$ .

The fact that these Mises strain concentrations are not observed at the two bottom layers is probably because of the bottom to top order of construction of the prism where bottom ones experience higher weight imposed by the upper bricks and mortar joints than the top layers. This induces more pressure and compaction for the bottom mortar layers mitigating the shear deformations caused by the mismatch effects.

#### 4 SOME REMARKS ON THE EXPERIMENTS AND THE DIC SYSTEM

The DIC system was employed throughout this study to observe and measure the full-field deformations of the specimens. Compared to the traditional way of using strain gauges which only measure extensional deformations at a limited number of discrete locations, the photogrammetry method used by the DIC system provides field information by measuring a very large number of data points dependent on the computation size, facet size and facet steps. It also captures in-plane and out-of-plane deformations simultaneously. Moreover, one of the main advantages of using the DIC system is measuring large deformations and strain concentrations on the surface of a specimen, while strain gauges often debond under large deformations. Therefore, in some studies which deal with large deformations like in damage or fracture mechanics, the DIC system is very useful to track deformations up to failure

On the other hand, the DIC system shows some inconsistencies in measuring small deformations in brittle materials like brick and mortars. For instance, for the three 14-day mortar cubes tested, the average chord young's moduli,  $E_{chord}$ , were 4518, 1857, and 7267 *ksi* showing no consistencies. The issue is much worse for the Poisson's ratio where the lateral horizontal strain,  $\epsilon_x$ , is much smaller than the vertical strain,  $\epsilon_y$ , causing erratic results in the linear stage which is determined based on the load-deformation curve of each specimen.

Figure 9 shows the distribution of lateral strain  $\epsilon_x$  contours on the surface of a brick

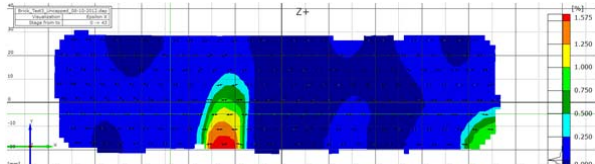


**Figure 9:** The distribution of  $\varepsilon_x$  contours on the surface of a brick at the linear behavior stage (73 kips or  $0.36P_{max}$ ).

tested in the linear range (73 kips or  $0.36P_{max}$ ). As it is seen, there are very different colors on the surface indicating large variations of the lateral strain values. Most of the points inside the darkest blue zone experience horizontal contraction or negative (compressive)  $\varepsilon_x$  in the brick in the linear elastic range which contradicts the Poisson's effect. The most probable reason for this phenomenon are the boundary conditions and the edge effects on the 2-inch high brick imposed by the testing machine platens on the top and bottom of the brick. It should be emphasized that these compressive zones would be ignored if no DIC system would be available. In the lighter blue zone, most points exhibit positive extensional values for the lateral  $\varepsilon_x$  strain.

Resolution issues of crack detection are one of the central issues for crack detection. A concise sensitivity analysis was conducted to evaluate the value of  $\varepsilon_x$  at failure at the location of the crack. Figure 10 depicts the distribution of  $\varepsilon_x$  along a section crossing the crack at failure in the masonry prism of Figure 7. It is seen that by changing the parameters of facet step or facet size the value of  $\varepsilon_x$  changes considerably. This means that the measured deformation around the crack by the DIC system is very sensitive with the post-processing parameters which must be considered when analyzing cracking data. In fact, the deformation measurement accuracy goes up as the facet size or facet steps increase. In Figure 10, the red solid line has the highest accuracy among other the curves having facet size and step of 35 and 32 pixels, respectively. The green solid line with small triangles has the lowest accuracy with the facet size and step of 20 and 18 pixels, respectively. It is observed that the sensitivity of  $\varepsilon_x$  to the facet step is larger than facet size as there is

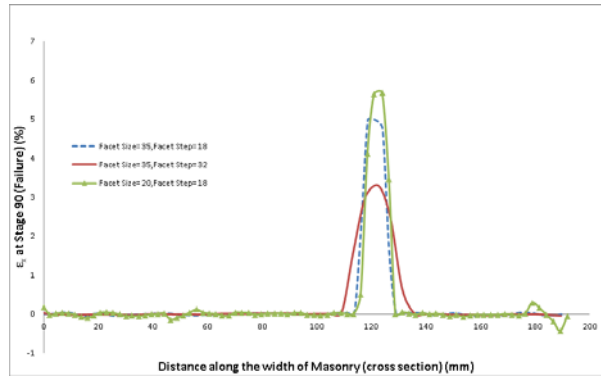


**Figure 10:** Distribution of  $\varepsilon_x$  along a section crossing the crack at failure ( $P_{max}$ ) in the masonry prism of Figure 7

more reduction in  $\varepsilon_x$  from facet step of 18 to 32 pixels (dashed blue line to solid red line).

Furthermore, as mentioned earlier, there are problems in measuring very small deformations and strains (usually less than 100 micro-strains) by the DIC system. This is more problematic for measuring lateral strains in axial testing, which is needed to calculate Poisson's ratio of interest. However, there is a built-in capability in ARAMIS to measure Poisson's ratio which is calculated as the ratio of the minor strain to the major principal strain. Figure 11 shows the distribution of Poisson's ratio values on the surface of the brick tested. In this case, the DIC furnished values which ranged from -10 to 10 as shown in the figure. However, it is better to use a filtration procedure to measure Poisson's ratio, if possible. Filtration techniques, removing edge effects, increasing the computation size, and selecting zones of data points on the surface of the specimen with uniform distribution of deformations and then averaging over zones without defects help to reach a realistic value. In fact, rational filtration of the raw data let to a Poisson estimate of 0.21 Nonetheless, great care must be taken in determining Poisson's ratio of brittle material like brick and mortar since the DIC system has to measure lateral strains

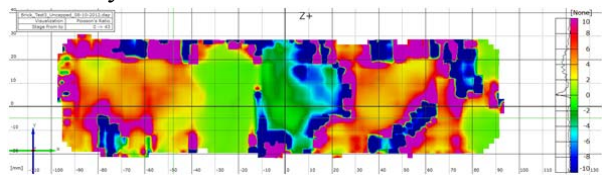


**Figure 11:** Poisson's ratio contours on the surface of the brick in Figure 9 measured by the DIC system.

which are smaller than the noise floor of the system. In other words, the resolution requires DIC measurements within the noise level.

## 5 CONCLUSION

The present study investigates the behavior of brick units, mortar cubes, and their assemblage as a five brick masonry prism under axial compression using the newly acquired digital image correlation system. Because of the deformation mismatch between stiffer brick and the softer mortar joints, the lateral tension in the brick units results in axial tensile splitting in the brick units when the masonry prism is under far-field axial compression. This tensile failure was observed in one of the experiments (Figure 7). Some other tests were performed on the constituents of a masonry prism. For both bricks and mortars some local response features like negative contractive lateral strain  $\varepsilon_x$  was captured by the DIC system on the surface of the specimen. It was postulated that these are mostly because of the boundary effects and imperfections especially in brick units as a sintered clay material. Moreover, it was mentioned that the DIC system measures real-time deformations during the test and provides at the end a crack pattern that closely matches that of the real specimen. This gives the DIC system an opportunity to provide feedback to the testing machine through measurement of the deformations in real-time. Final remarks on the experiments and the DIC system referred to the spatial resolution of small deformation measurement at the noise floor of the system through the effect of facet size and facet steps, and the time resolution through the computation step size.

Employing the DIC capability of real-time measurement could be a robust tool to study the behavior of a crack and its propagation in a masonry prism or its constituents or generally the post-peak behavior of the composite material. A numerical nonlinear finite element analysis can be bundled with the experimental results obtained by DIC in order to penetrate the subtle interaction effects of brittle-ductile transition in dependence of interface bond. In this sense, the capability of comparing predictions of Finite Element Analysis

(FEA) with DIC data may be utilized for quantitative verification and validation studies. Future research, could address the numerical issue of snap-back instabilities in the case of softening of thin mortar layers between elastic brick units. There the question is still wide open whether tensile cracking of the masonry prism under axial compression precedes emerging snap-back instabilities in the composite, or whether tensile cracking of the brick units is the result of the energy release during snap-back.

## ACKNOWLEDGMENT

The authors would like to acknowledge the support of this research effort by the US National Science Foundation. Opinions expressed in this paper are those of the authors and do not necessarily reflect those of the sponsor.

## REFERENCES

- [1]. **Goodman, R., Taylor, R, Brekke, L. A** Model for the Mechanics of Jointed Rock. *Journal of the Soil Mechanics and Foundations Divisions, Proceedings of the American Society of Civil Engineers*. 1968, Vol. 94, SM3, pp. 637-659.
- [2]. **Page, Adrian W.** Finite Element Model for Masonry. *Journal of the Structural Division*. 1978, Vol. 104, 8, pp. 1267-1285.
- [3]. **McNary, W., Abrams, D.** Mechanics of Masonry in Compression. *Journal of Structural Engineering*. 1985, Vol. 111, 4, pp. 857-870.
- [4]. **Sarangapani, G., Reddy, BV Venkatarama, Jagadish, KS.** Brick-Mortar Bond and Masonry Compressive Strength. *Journal of Materials in Civil Engineering*. 2005, Vol. 17, 2, pp. 229-237.
- [5]. **Blackard, B., Kim, B., Citto, C., Willam, K., Mettupalayam, S.** Experimental Observations of Masonry Infilled Reinforced Concrete Frames with Openings. *Fracture Mechanics of Concrete and Concrete Structures- High Performance Concrete*,

*Brick-Masonry and Environmental Aspects.*  
2007, pp. 1587-1594.

[6]. **Willam, K., Blackard, B., Citto, C.**  
Failure Studies on Masonry Infill Walls:  
Experimental and Computational  
Observations. *Proc. Euroc 2010 on  
Computational Modelling of Concrete  
Structures.* 2010, pp. 757-765 .

[7]. **Citto, C., Wo, S.I., Willam, K., Schuller,  
M.P.** In-Place Evaluation of Masonry  
Behavior Using Digital Image Analysis. *ACI  
Materials Journal.* 2011, Vol. 108, 4, pp. 413-  
422.

[8]. **ARAMIS System.** ARAMIS User  
Manual-Software. Braunschweig, Germany :  
GOM GmbH, 2011.

[9]. **ASTM.** Standard Test Method for  
Splitting Tensile Strength of Masonry Units.  
Philadelphia : American Society for Testing  
and Materials, 2001. ASTM C 1006-84.

[10]. **ASTM.** Standard Test Method for  
Compressive Strength of Masonry Prisms.  
Philadelphia : American Society for Testing  
and Materials, 2003. ASTM C 1314 – 03b.